New insights into the involvement of residue D1/V185 in Photosystem II function in *Synechocystis 6803* and *Thermosynechococcus vestitus*.

Alain Boussac[a], Julien Sellés[b], Miwa Sugiura[c], Robert L. Burnap[d]

[a] Institut de Biologie Intégrative de la Cellule, UMR9198, CEA Saclay, 91191 Gif-Sur-Yvette, France. alain.boussac@laposte.net

[b] Institut de Biologie Physico-Chimique, UMR CNRS 7141 and Sorbonne Université, 13 rue Pierre et Marie Curie, 75005 Paris, France. julien.selles@ibpc.fr

[c] Proteo-Science Research Center, Department of Chemistry, Graduate School of Science and Technology, Ehime University, Bunkyo-cho, Matsuyama, Ehime 790-8577, Japan. miwa.sugiura@ehime-u.ac.jp

[d] Department of Microbiology and Molecular Genetics, Oklahoma State University, Stillwater, OK 74078. rob.burnap@okstate.edu

ORCID numbers :

Alain Boussac: 0000-0002-3441-3861

Miwa Sugiura: 0000-0002-4232-5941

Julien Sellés: 0000-0001-9262-8257

Robert L. Burnap: 0000-0001-6715-5961

Key words :

Photosystem II, D1-V185, EPR, proton release, S-state cycle, spin state, Mn_4CaO_5 cluster

Abbreviations:

Photosystem II, PSII; Chl, chlorophyll; Chl_{D1}/Chl_{D2}, monomeric Chl on the D1 or D2 side, respectively; MES, 2-(*N*-morpholino) ethanesulfonic acid; P_{680}, primary electron donor; P_{D1} and P_{D2}, individual Chl on the D1 or D2 side, respectively, which constitute a pair of Chl with partially overlapping aromatic rings; Phe_{D1} and Phe_{D2}, pheophytin on the D1 or D2 side, respectively; PPBQ, phenyl *p*–benzoquinone; Q_A, primary quinone acceptor; Q_B, secondary quinone acceptor; Tyr_Z, the tyrosine 161 of D1 acting as the electron donor to P_{680}; WT*3, *T. elongatus* mutant strain deleted *psbA1* and *psbA2* genes and with a His-tag on the carboxy terminus of CP43. EPR, Electron Paramagnetic Resonance. ML, multiline.

Abstract

The effects of D1-V185T and D1-V185N mutations in Photosystem II (PSII) from *Thermosynechococcus vestitus* (formerly *T. elongatus*) and *Synechocystis* 6803, respectively, were studied using both EPR and optical kinetics. EPR spectroscopy reveals the presence of a mixture of a S_2 state in a high spin configuration (S_2^{HS}) and in a low spin configuration (S_2^{LS}) in both mutants. In contrast to the S_2^{HS} in the wild type, the S_2^{HS} state in the D1-V185T mutant does not progress to the S_3 state at 198 K. This inability is likely due to alterations in the protonation state and hydrogen-bonding network around the Mn_4CaO_5 cluster. Optical studies show that these mutations significantly affect proton release during the S_3-to-S_0 transition. While the initial fast proton release associated with $Tyr_Z^{\bullet}$ formation remains unaffected within the resolution of our measurements, the second, and slower, proton release is delayed, suggesting that the mutations disrupt the hydrogen-bonding interactions necessary for efficient deprotonation of substrate water (O6). This disruption in proton transfer also correlates with slower water exchange in the S_3 state, likely due to non-native hydrogen bonds introduced by the threonine or asparagine side chains at position 185. These findings point to a critical role of D1-V185 in regulating both proton transfer dynamics and water binding, underscoring a complex interplay between structural and functional changes in PSII.

Introduction

Oxygenic photosynthesis in cyanobacteria, algae and higher plants converts solar energy into the chemical bonds of sugars and oxygen [1]. Photosystem II (PSII) begins this process by splitting water to obtain electrons in the form of reduced quinone, while generating a proton gradient and releasing O_2. The mature PSII binds 35 chlorophylls *a* (Chl-*a*),two pheophytins (Phe-*a*), one membrane b-type cytochrome, one extrinsic c-type cytochrome (in cyanobacteria and red algae), one non-heme iron, two plastoquinones (Q_A and Q_B), the Mn_4CaO_5 cluster, 2 Cl^-, 12 carotenoids and 25 lipids [2,3]. In the cyanobacterium *Synechocystis sp.* PCC 6803 a 4th extrinsic subunit, PsbQ, has also been found in addition to PsbV, PsbO and PsbU [4].

Among the 35 Chl-*a*, 31 are antenna Chls. When one is excited, the excitation energy is transferred to other chlorophylls until it reaches the key pigments in the photochemical reaction center: 4 Chl-*a* molecules, P_{D1}, P_{D2}, Chl_{D1}, Chl_{D2} and 2 Phe-*a* molecules, Phe_{D1} and Phe_{D2}. A few picoseconds after the formation of the excited $^*Chl_{D1}$, charge separation occurs, ultimately forming the $Chl_{D1}^+Phe_{D1}^-$ and then $P_{D1}^+Phe_{D1}^-$ radical pair states, *e.g.* [5,6]. Formation of the $Chl_{D1}^+Phe_{D1}^-$ radical pair was recently defined as a fast pathway (short-range charge-separation) in contrast with a slow pathway with $P_{D1}P_{D2}$ as the initial donor (long-range charge separation) that would result directly in the formation of the $P_{D1}^+Phe_{D1}^-$ radical pair [7].

After the charge separation, P_{D1}^+ oxidizes Tyr_Z, the Tyr161 of the D1 polypeptide, which is then reduced by the Mn_4CaO_5 cluster. The electron on Phe_{D1}^- is then transferred to Q_A, the primary quinone electron acceptor, and then to Q_B, the second quinone electron acceptor. Whereas Q_A can be only singly reduced under normal conditions, Q_B accepts two electrons and two protons before leaving its binding site and being replaced by an oxidized Q_B molecule from the membrane plastoquinone pool, see for example [1,8–12] for a non-exhaustive list of recent reviews on PSII function. The Mn_4CaO_5 cluster, oxidized by the $Tyr_Z^\bullet$ radical formed after each charge separation, cycles through five redox states denoted Sn, where n designates the number of stored oxidizing equivalents. The S_1 state is stable in the dark, which makes S_1 the preponderant state after the decay of the S_3 and S_2 states in the dark. When the S_4 state is formed, after the 3rd flash of light given on dark-adapted PSII, two water molecules bound to the cluster are oxidized, O_2 is released and the S_0-state is reformed, [13,14].

Thanks to the advent of serial femtosecond X-ray free electron laser crystallography and cryo-EM spectroscopy, structures of the Mn_4CaO_5 cluster have been resolved in the dark-adapted S_1 state, the S_2 and S_3 states, in a redox state as close as possible to those expected taking into account the misses under flash illumination. In the S_1 state, *i.e.* in the $Mn^{III}{}_2Mn^{IV}{}_2$ redox state, the Mn_4CaO_5 structure resembles a distorted chair, including a μ-oxo-bridged cuboidal Mn_3O_4Ca unit with a fourth Mn attached to this core structure *via* two μ-oxo bridges involving the two oxygen's O4 and O5 [2]. Recently, important progress has been made in the resolution of the crystal structures in the S_2, S_3 [15-17] and S_0 states [15,16]. Briefly, changes in the S_1 to S_2 transition more or less correspond to those expected for the valence change of the Mn4 from +III to +IV. Importantly, water molecules in the "O1" and "O4" channels, defined as such because they start from the O1 and O4 oxygens of the cluster, appeared localized slightly differently in S_2 and S_1. In contrast, in the S_2 to S_3 transition, major structural changes have been detected together with the insertion of a 6th oxygen (named either O6 or Ox), possibly that one of W3 originally bound to the Ca site, bridging Mn1 and Ca. This oxygen is supposed to correspond to the second water substrate molecule and is close to the bridging oxygen O5 supposed to be the first water substrate molecule [18]. An important movement of the Glu189 residue would allow its carboxylate chain to make a hydrogen bond with the protonated form of the 6th oxygen in S_3 [16,17].

EPR data studies show the existence of multiple structural forms for each of the S_1, S_2, and S_3 states. The S_1 EPR signals seen with a parallel mode detection at $g \sim 4.8$ and $g \sim 12$ [19–21] were attributed to an orientational Jahn–Teller isomerism of the dangler Mn4 with the valence +III [22].

In S_2, at least two EPR signals can be detected at helium temperatures. The first one has a low-spin $S = 1/2$ value, S_2^{LS}, characterized by a multiline signal (ML) made up of at least 20 lines separated by approximately 80 gauss, centered at $g \sim 2.0$ and spread over roughly 1800 gauss [23–25]. The second configuration of S_2 is a high-spin ground state, S_2^{HS}, with $S \geq 5/2$. In plant PSII, S_2^{HS} may exhibit either a derivative-like EPR signal centered at $g \sim 4.1$ [26,27] or more complex signals at higher g values [28,29]. In cyanobacterial PSII, the $g \sim 4.1$ signal is not detected. Instead, the S_2^{HS} EPR signal has a derivative-like shape centered at $g \sim 4.8$ [30,31].

An influential computational study proposed that the $g \sim 4.1$ signal has almost the same coordination and environment as the $g \sim 2.0$ ML signal, but with the Mn^{III} ion located on the dangler Mn4 in the S_2^{HS} state instead on the Mn1 in the S_2^{LS} state [32]. This valence swap would be accompanied by a moving of the oxygen O5 from a position where it links the

Mn4, Mn3 and the Ca in the S_2^{LS} configuration to a position where it bridges the Mn1, Mn3, and Ca ions in the S_2^{HS} configuration resulting in the so-called closed cubane structure. However, this proposed closed cubane structure for the S_2^{HS} configuration has never been observed by XFEL studies of PSII, either from plants or cyanobacteria, in conditions where the S_2^{HS} is known to be trapped at low temperatures. For cyanobacteria, this result is not surprising since in this PSII the $g \sim 4.1$ signal has never been observed until now. Yet, it remains possible that the proposed configuration is a short-lived transient that the time-resolved studies have not captured due to limited post-flash sampling frequency.

On the other hand, other computational works [33-35] led to a different model, that, starting from the S_2^{LS} configuration, the protonation of O4 would lead to an $S = 5/2$ ground state when W1, one of the two water molecules with W2 bound to the dangler Mn4, is present as an aquo ligand. The further deprotonation of W1 to form a hydroxo ligand would then give rise to an $S = 7/2$ ground state [33-35]. It was further proposed that the form $S = 7/2$ was required to progress to S_3. Importantly, the S_2^{HS} form detected at $g \sim 4.8$ form, *i.e.* the $S = 7/2$ form, that corresponds to an open cubane structure in [33-35], is able to progress to S_3 at low temperatures [30,31], whereas in plant PSII the $g \sim 4.1$ state cannot [36].

The S_3-state also exhibits some heterogeneities based on EPR analysis. Most centers exhibit a spin $S = 3$ ground state [37-39]. In this $S = 3$ configuration, the four Mn ions of the cluster have an Mn^{IV} formal oxidation state with an octahedral ligation sphere in an open cubane structure [39]. In this model, the dangler Mn^{IV} ($S = 3/2$) is antiferromagnetically coupled to the open cubane motif Mn^{IV}_3 with a total spin value $S = 9/2$. The remaining centers are EPR invisible, *e.g.* [40]. A third S_3 configuration with a broadened S_3 signal was identified with ELDOR-detected NMR (EDNMR) in the presence of glycerol [41,42] and in PSII/Sr [43]. Although in [43] the authors did not completely rule out the presence of a closed cubane, five-coordinate S_3 form, at the origin of this EPR signal, they favored a perturbation of the coordination environment at Mn4 and/or Mn3 in an open cubane S_3 structure induced by glycerol. With X-and Q-band EPR experiments performed in the S_3-state of plant PSII, both in the perpendicular and parallel modes, a high-spin, $S = 6$, was proposed to coexist with the $S = 3$ configuration. This $S = 6$ form was attributed to a form of S_3 without O6/Ox bound and with the Mn^{IV}_3 part of the cluster in ferromagnetic interaction with the unsaturated dangler Mn^{IV} [42]. These two forms of S_3 are, however, not detected by X-band EPR, so it seems unlikely that they correspond to the EPR invisible S_3 mentioned above. Indeed, these new S_3 signals described in [41,42] are detectable in the presence of glycerol and methanol, whereas the formation of the $(S_2Tyr_Z^{\bullet})'$ state upon a near-IR illumination in the centers in S_3 defined as

EPR invisible is inhibited in the presence of glycerol (and in the presence of methanol in plant PSII) [44,45].

In cyanobacterial PSII/Sr [43], a proportion of centers exhibited a pulsed W-band field-swept S_3 spectrum much broader than in PSII/Ca. This signal was proposed to be present in centers containing a 5-coordinate Mn ion in centers in which no water binding event takes place during the S_2 to S_3 transition. It was therefore proposed that, in these centers, the oxidation event would precede the water binding. Computational analyses also suggested heterogeneities in S_3 [46–48] with also a $S = 6$ spin value [48].

None of the heterogeneities described above were detected in the crystallographic structures of S_2 and S_3 known to date (see references above). In addition, recent high-energy resolution fluorescence detected X-ray Absorption Spectroscopy together with QM calculations ruled out the presence of either peroxo or oxo/oxyl level intermediate to explain the S_3 heterogeneity [49].

It is quite possible that some of the structural differences that cause the differences identified in EPR are too small to be detectable given the resolution of the crystallographic data. This at least shows, if it were necessary, that spectroscopy remains an indispensable complement to crystallography.

The EPR data summarized above describes a static view of the trapped configurations. Kinetically, it is well documented that the transition from S_2 to S_3 involved at least two phases. The fastest phase, with a $t_{1/2} \leq 25$ µs, is attributed to a proton transfer/release. This fast phase precedes the electron transfer from S_2 to the $Tyr_Z^{\bullet}$ occurring with a $t_{1/2} \leq 300$ µs [50–54], and the binding of O6/Ox to the Mn1, *e.g.* [55]. It was proposed that the fast phase could correspond to the release of a proton in an intermediate step $S_2^{LS}Tyr_Z^{\bullet} \rightarrow S_2^{HS}Tyr_Z^{\bullet}$ before the $S_2^{HS}Tyr_Z^{\bullet} \rightarrow S_3^{S=3}$ transition occurs [30]. The existence of intermediate states in the S_2 to S_3 transition was tracked by following, at room temperature, the structural changes in the S_2 to S_3 transition in the µs to ms time-range after the 2nd flash [17,55]. No indication was found for a closed cubane intermediate. However, there was no conclusion on the spin state of the intermediate forms of S_2 able to progress to S_3. By definition, an intermediate state has a low concentration that makes its detection difficult and thus, the question of the existence of a high spin intermediate state in the S_2 to S_3 transition remains. It is possible that the S_2^{HS} corresponds to a subtle structural/tautomeric intermediate that nonetheless mediates proton release during the $S_2^{LS}Tyr_Z^{\bullet} \rightarrow S_2^{HS}Tyr_Z^{\bullet}$ as a prerequisite to the formation of the S_3 $S = 3$ state. It has been suggested that the fast phase observed in this transition corresponds to a proton release/movement associated with the formation of a S_2^{HS} state [30,36]. If this is

correct, we would expect to detect a change in the flash pattern of the proton release in conditions in which the S_2^{HS} EPR signal is the flash-induced state. This was indeed the case since we have kinetically detected a proton release in PSII/Ca and PSII/Sr at pH 6.0 and 7.0, knowing that at pH 7.0, in PSII/Sr in contrast to PSII/Ca, half of the centers exhibit the S_2^{HS} signal at g ~ 4.8 able to progress to S_3 at low temperatures [36].

Independently of the pH effect and Ca/Sr exchange, several mutations, the list being too long for making it here, in the first and second coordination sphere of the Mn_3O_4Ca unit strongly perturb the water splitting process. One of these mutants is the D1/V185N mutant in *Synechocystis* 6803 [56-59]. The D1/V185 residue is located adjacent to the cluster near three potential substrate candidates (W2, W3 and O5). It may also block or regulate the access to the open coordination site at Mn1. The D1/V185N mutation in *Synechocystis* sp. PCC 6803 slows down the release of O_2 from 1.2 ms to about 27 ms halftime at 27 °C. In addition, the rate of exchange for the slower exchangeable water substrate molecule, Ws, was increased in the S_1 and S_2 states in the D1/V185N mutant, while both Wf, the faster exchangeable water substrate molecule, and Ws exchange rates were decreased in the S_3 state in this mutant [59]. In contrast to the situation in the V185T mutant in *Synechocystis* 6803 in which the oxygen release kinetics was hardly affected (from 1.2 ms to 1.5 ms) [57], the D1/V185T mutation in *T. vestitus* resulted in similar phenotype to those in the D1/V185N in *Synechocystis* sp. PCC 6803 [60].

In the D1-V185T mutant in *T. vestitus* we found that the S_2 state was mostly present in a high spin configuration [60] although a modified multiline was also observed. This observation triggered us to probe the proton release in the S_1 to S_2 transition in the context of the model mentioned above where the proton released in the S_2 to S_3 transition occurs in the $S_1Tyr_Z^{\bullet} \rightarrow S_2^{HS}Tyr_Z^{\bullet}$ transition prior to the $S_2^{HS}Tyr_Z^{\bullet}$ to S_3 transition [30,36]. One of the problem here is that measuring the proton release kinetics by using a dye as we did in [60] required an extensive washing of the PSII samples to remove all the buffers, a treatment that has deleterious effects on the particularly fragile D1/V185T mutant. In so doing, we observed a rapid phase of proton release into the bulk, the kinetics of which was close, and difficult to distinguish from that observed following oxidation of Tyr_Z at pH 6.3 in Mn-depleted PSII. To get around this problem, we also measured the electrochromic band shifts induced by each of the flashes in a sequence that is an alternative way to follow the movement of the charges in and around the Mn_4CaO_5 cluster [36,54].

As the μs components kinetics in the P_{680}^{+} reduction reflect the progressive shift to the left of the equilibrium $P_{680}^{+}Tyr_Z \leftrightarrow P_{680}Tyr_Z^{\bullet}$ resulting from slower proton release/movements [61-63], we also measured the P_{680}^{+} decay in the D1/V185T mutant in *T. vestitus*.

Recently [59], it was reported that the high spin EPR signal in the S_2 state of the D1/V185N PSII in *Synechocystis* 6803 was not detectable. We report here, in an independent EPR experiment, that the S_2^{HS} EPR signal in the D1/V185N PSII from *Synechocystis* 6803 is clearly present. This combined with the retardation in the S_n state transition reaction kinetics, now provides a consistent picture of the effects mutations at this second sphere location and reinforces criticality of the H-bonding network in in mediating the catalysis of water oxidation.

Materials and methods

Purification of the D1-V185N mutant from *Synechocystis 6803* was previously described in [56]. The D1 protein is PsbA2 in this mutant strain. Purification of the D1/V185T mutant from *T. vestitus* was previously described in [60]. The D1/V185T mutant has been constructed in the *psbA3* gene so that the wild type PSII is that one with PsbA3.

Time-resolved absorption changes measurements were performed with a lab-built spectrophotometer [64] slightly modified as described in detail in [65]. For the ΔI/I measurements the samples were diluted in 1 M betaine, 15 mM $CaCl_2$, 15 mM $MgCl_2$, and 40 mM MES (pH 6.5). PSII samples were dark-adapted for ~1 h at room temperature (20–22°C) before the addition of 0.1 mM phenyl *p*–benzoquinone (PPBQ) dissolved in dimethyl sulfoxide. The chlorophyll concentration of all the samples was ~ 25 μg of Chl mL^{-1}. After the measurements, the ΔI/I values were normalized to exactly *A*673 = 1.75, that is very close to 25 μg Chl mL^{-1}. The measurements with the dye bromocresol purple were done as previously reported after the removal of Mes [36].

X-band cw-EPR spectra were recorded with a Bruker Elexsys 500 X-band spectrometer equipped with a standard ER 4102 (Bruker) X-band resonator, a Bruker teslameter, an Oxford Instruments cryostat (ESR 900) and an Oxford ITC504 temperature controller. The samples, at ~ 1.35 mg Chl mL^{-1}, were dark-adapted for 1 h on ice then the samples were frozen in the dark (without any addition) to 198 K in a dry-ice/ethanol bath and then transferred into liquid N_2 (77 K). Prior to recording the spectra, the samples were degassed at 198 K. The S_2 state was induced by illumination with an 800 W tungsten lamp

filtered by water and infrared cut-off filters for approximately 5–10 s at 198 K in a non-silvered Dewar in ethanol cooled with dry ice.

Results

As the interpretation of the data strongly depends on the presence of an S_2^{HS} state in the D1/V185N mutant in *Synechocystis* 6803, something that was contested in [59], we will firstly show the EPR spectra recorded in this strain. Fig. 1 compares the spectra in the PSII from *Synechocystis* 6803 WT (Panel A), and from the *S* 6803 D1/V185N-PSII (Panel B). The black spectra were recorded in the dark-adapted samples, the red spectra after continuous illumination at 198 K for 5-10 s, and the blue spectra are the light-*minus*-dark difference spectra.

In the WT sample (Panel A) the light-induced state exhibits a normal S_2^{LS} multiline signal similar to that induced in plant PSII and cyanobacterial PSII [10]. In contrast, in the D1/V185N PSII (Panel B), the shape and the amplitude of the multiline signal differs significantly from that one in the WT PSII. The S_2 multiline signal in the D1/V185N sample is very similar, if not identical, to the S_2 multiline signal in the D1/V185T mutant in *T. vestitus* [60]. Importantly, a large S_2^{HS} EPR signal, centered at ~ 1700 gauss, was induced by the illumination at 198 K in the D1/V185N mutant. This S_2^{HS} EPR signal is also virtually identical to the S_2^{HS} EPR signal detected in the D1/V185T mutant in *T. vestitus* [60].

In the black and red spectra other signals are detected. The g_z and g_y of Cytc_{550} are detected at ~ 2300 and ~ 3000 gauss, respectively. The two small negative signals in the blue spectra, between ~ 800 and ~ 1000 gauss, correspond to the negative non-heme iron signal. This means that the non-heme iron was oxidized in a proportion of centers in the dark-adapted state and reduced by the Q_A^- formed by the illumination at 198 K [66]. The large narrow signal at around 1600 gauss is due to contaminating Fe^{3+}. In both samples, the g ~ 1.9 form of the $Q_A^-Fe^{2+}Q_B$ signal (~ 3700 gauss) and the $Q_A^-Fe^{2+}Q_B^-$ signal at g ~ 1.6 (~ 4400 gauss) are detected. The change in their relative proportion is likely due to a different proportion of the $Q_AFe^{2+}Q_B^-$ state in the dark adapted samples. In the black spectra, the $Q_AFe^{2+}Q_B^-$ signal is possibly present at ~ 4200 gauss and indeed larger in the mutant, *i.e.* [67].

In conclusion, an unequivocally similar S_2^{HS} EPR signal is formed in the D1/V185N PSII from *Synechocystis* 6803 and the D1/V185T PSII mutant from *T. vestitus* mutant [60].

Knowing with certainty that both mutants exhibit an S_2^{HS} state at pH 6.5, the question about a proton release into the bulk in the S_1 to an S_2 state with such S_2^{HS} EPR properties

should be addressed again. Firstly by measuring the proton/release using the dye bromocresol purple. Secondly by recording the electrochromic band-shifts in the Soret region of the P_{D1} absorption spectrum at 440 nm. Indeed, this measurement takes into account both the proton uptake/release and the electron transfer events, *e.g.* [54,68] and references therein. In addition, unlike the situation with the dyes, the electrochromism is not contaminated by the protonation/deprotonation events coupled to the reduction/oxidation of the non-heme iron. For the removal of the contributions due to the reduction of Q_A the ΔI/I at 424 nm was also measured. Indeed, the electrochromism due to Q_A^- equally contributes at 440 nm and 424 nm [68]. These measurements can be compared to the proton uptake/release kinetics again measured with bromocresol purple as in [60].

Panels A and B in Fig. 2 shows the absorbance changes of bromocresol purple in PsbA3-PSII and PsbA3/V185T-PSII, respectively, both from *T. vestitus*. An uptake of protons by PSII induces an increase in the ΔI/I at 575 nm, and a release of protons into the bulk by PSII induces a decrease of the ΔI/I. After the first flash (black points), there was a large increase in the absorption in both samples. This increase is due to the proton uptake following the reduction of the non-heme iron [36]. In PsbA3-PSII (Panel A) there is no detectable proton release associated with the S_1 to S_2 transition as already seen in such a PsbA3-PSII [36]. This is consistent with a large body of experiments indicating the absence of proton release in this transition, and with a 1-0-1-2 pattern of proton release for the S_0 to S_1, S_1 to S_2, S_2 to S_3 and S_3 to S_0 transitions, reviewed in [36,56]. In contrast with our previous study [60], however, the decrease in the ΔI/I in the 10 µs to 100 µs time range is very small, suggesting that a proton release, if any, occurs in a very low proportion of the centers. This lack of proton release is very likely due to the use of a PsbA3/V185T-PSII sample less damaged by the washing steps compared to the earlier study. Additionally, proton uptake is detected after each flash as previously reported [36] explaining the drift in the signal (not subtracted in Panels A and B) observed on each flash. The proton release kinetics in the PsbA3/V185T-PSII in the S_2 to S_3 transition (red points) and in the S_0 to S_1 transition (green points) appears hardly affected when compared to PsbA3-PSII (~ 30-40 µs, and ~ 100-200 µs, respectively). In the S_3 to S_0 transition, the release of the first proton is also hardly affected in the mutant. In contrast, the release of the second proton is strongly slowed down with a kinetics similar to the O_2 release (~ 20-30 ms) [56,60].

Panel C in Fig.2 shows the kinetics of the 440 nm-*minus*-424 nm difference in the PsbA3/V185T-PSII from *T. vestitus*. The results can be compared to those obtained in PsbA3-PSII that have been described in details previously [36,54]. After the first flash (black points),

the kinetics that corresponds to the $S_1Tyr_Z^{\bullet}$ to the S_2Tyr_Z transition is slightly slowed down from 10-20 µs to 50-60 µs in the PsbA3/V185T mutant. After the second flash (red points) the kinetics is biphasic with a fast phase ($t_{1/2}$ ~ 10-15 µs) that we have attributed to a proton movement coupled to the $S_2^{LS}Tyr_Z^{\bullet}$ to $S_2^{HS}Tyr_Z^{\bullet}$ transition, and the slow phase was attributed to the $S_2^{HS}Tyr_Z^{\bullet}$ to the S_3Tyr_Z transition [36]. In the PsbA3/V185T-PSII mutant the two phases are not really differentiated, which makes the interpretation difficult even if this result could suggest a slowing down of the proton release in the S_2 to S_3 transition. In the PsbA3-PSII, after the fourth flash, the kinetics is also biphasic with the fast phase corresponding to the electron transfer in the S_0 to S_1 transition ($t_{1/2}$ ~ 10-15 µs), which precedes the proton release with a $t_{1/2}$ ~ 200 µs [36,50,54]. In the PsbA3/V185T-PSII, after the fourth flash (green points), although the two phases are also difficult to be detected due to a less good signal-to-noise ratio, and an increase miss parameter (see however below), the two phases seem to have more or less the same kinetics. The big difference between Panel A and Panel B is the slow phase after the third flash (blue points) with a $t_{1/2}$ ~ 20-30 ms in D1/V185T-PSII, which is similar to that of the proton release in this sample. After the 4th flash the slow decay certainly originates from a residual S_3 to S_0 transition due to the misses but we have no clear explanation for the slow drift after the 1st and 2nd flash since the redox events at the non-heme iron do not contribute in the electrochromism of P_{D1}.

Each event, such as a change in the kinetics of electron and proton motion, should affect the $P_{680}^{+}Tyr_Z \leftrightarrow P_{680}Tyr_Z^{\bullet}$ equilibrium and therefore the P_{680}^{+} decay kinetics. Panels A, B, C, and D in Fig. 3 show the P_{680}^{+} reduction kinetics measured at 432 nm in PsbA3-PSII (black), and PsbA3/V185T-PSII (red) after the 1st flash (Panel A), the 2nd flash (Panel B), the 3rd flash (Panel C) and the 4th flash (Panel D). In all the S_n states, the decay of P_{680}^{+} in the PsbA3/V185T mutant is significantly slower both in the ns time-domain corresponding to the pure electron transfer step, and the µs time-domain where the electron transfer(s) is(are) coupled to proton movements. The $P_{680}^{+}Tyr_Z \leftrightarrow P_{680}Tyr_Z^{\bullet}$ is therefore shifted to the left in the PsbA3/V185T mutant when compared to the PsbA3-PSII in all the S_n states [61,63] and we expect that some of the proton movements coupled to the electron transfer are also slowed down.

Panel E in Fig. 3 shows the ΔI/I measured 20 ns after each flash of the sequence in the PsbA3-PSII (black) and in the PsbA3/V185T-PSII (red). Due to the slower decay of P_{680}^{+} in the S_2 and S_3 states [69] than in the S_0 and S_1 states we obtain an oscillation with the period of four. Since in all the S_n states the decay of P_{680}^{+} is faster in PsbA3-PSII than in PsbA3/V185T-

SII, the ΔI/I values in PsbA3-PSII, 20 ns after the flashes, are smaller (less negative) in all the S_n states. However, the oscillations are similar in both samples, which indicates that in the PsbA3/V185T-PSII used here the miss parameter is not significantly larger than in the PsbA3-PSII.

Discussion

One of the main results shown in this work is the presence of a S_2^{HS} in the D1/V185N-PSII from *Synechocystis* 6803, with EPR characteristics strikingly similar to those observed in the D1/V185T-PSII mutant from *T. vestitus* [60]. The discrepancy between the EPR spectra shown here and those in [59] is likely attributable to baseline distortions in the low-field region of the spectra in [59]. Such distortions hinder the clear detection of the S_2^{HS} signal. By addressing this technical issue, we demonstrate the consistent appearance of the S_2^{HS} state in these mutants, reinforcing the idea that the D1/V185 residue influences the high-spin/low-spin equilibrium of the S_2 state in a similar manner across different cyanobacterial species and supports a consistent mechanism by which a perturbation of this site modulates the still enigmatic S_2^{HS} state in PSII. Because these are substitutions of a hydrophobic with polar residues, they introduce H-bonding potential at a location adjacent to the insertion point of substrate water O_6/O_x that arrives at the open coordination position of Mn1 during the $S_2 \rightarrow S_3$ transition. Thus, the mutations almost certainly exert their effects by introducing aberrant H-bonding interactions that compete and thus perturb the native H-bond network, which has been evolutionarily optimized to enhance catalytic efficiency. The inferred mutational perturbation of native H-bonding may thus be at the basis of some of the observed EPR and kinetic alterations as discussed below.

It has been shown that the equilibrium between the S_2^{LS} and S_2^{HS} states is pH dependent [30], with a $pK_a \sim 8.3$ for the native Mn_4CaO_5 cluster and a significantly shifted pK_a of ~ 7.0 for the Mn_4SrO_5 cluster [36]. Alkaline conditions are thought to mimic the charged state of the $Tyr_Z^{\bullet}$, emulating the electrostatic proton ejection regime that facilitates progression through the Kok cycle [30,36,50,51,70,71]. Furthermore, there is some evidence that the Mn_4CaO_5 must pass through an S_2^{HS} intermediate state before forming the S_3 state. For example, the S_2^{HS} state formed by the room temperature flash illumination could progress to S_3 under further continuous illumination at 198 K. Similarly, samples advanced to the S_2^{LS} state upon illumination at 198 K subsequently form the S_2^{HS} state when warmed to room temperature, enabling progression to the S_3 state under further illumination at 198 K. These

observations have led to the tentative conclusion that the S_2^{HS} state is a necessary intermediate during the $S_2 \rightarrow S_3$ transition.

The lowered pK_a of the Mn_4SrO_5 cluster explains why the S_2^{HS} to S_3 transition can occur in a significant proportion of centers even at pH 6.5. Interestingly, D1/V185T-PSII also exhibits a high proportion of centers with an S_2^{HS} signal at pH 6.5, suggesting that these centers could progress to the S_3 state under illumination at 198 K. However, this progression is not at all evident in D1/V185T-PSII with a Mn_4CaO_5 cluster, as shown in spectrum *a* of Fig. 9 in [60]. In contrast, in D1/V185T-PSII with a Mn_4SrO_5 cluster, the effect of the 198 K illumination was more pronounced (spectrum *b* in Fig. 9 in [60]). However, the S_2^{HS} EPR signal that disappeared in D1/V185T-PSII with a Mn_4SrO_5 cluster upon the 198 K illumination had a shape similar to that in the wild type PSII (with both Ca and Sr in the cluster). This observation suggests some heterogeneity in the EPR properties of the S_2^{HS} state in D1/V185T-PSII with a Mn_4SrO_5 cluster. Importantly, since the illumination at 198 K results in the formation of the S_2^{HS} and S_2^{LS} states in both species, it seems likely that each of these two states arises from two structurally different S_1 states.

The previously mentioned possibility [60] for a S_2^{HS} to S_3 transition occurring at 198 K in D1/V185T-PSII seemed to be supported by the detection of a proton release on the first flash, see [36]. However, it is shown here that this proton release does not occurs in active D1/V185T-PSII but rather as originating from the oxidation of Tyr_Z in a minor sub-population Mn-depleted centers in the D1/V185T-PSII used for proton release experiment in [60]. It can now be concluded that the S_2^{HS} state in D1/V185T-PSII, with EPR properties different from those in wild type PSII, is unable to progress to S_3 at 198 K, most likely because its protonation state differs.

The S_2^{HS} EPR signal in the D1/V185T-PSII from *T. vestitus*, and the D1/V185N-PSII from *Synechocystis* 6803, have a shape reminiscent of the spectrum induced by near-infrared illumination of the S_2^{HS} state at high pH in PsbA3-PSII see Fig. 3 in [72]. Presently, there is no explanation of the near-infrared illumination however this similarity could suggest that the two states only differ by small structural changes, such as shifts in the H-bonding and proton tautomer configurations.

Functionally significant hydrogen bonding changes due to mutations at D1/V185 likely affect the stabilization and dynamics of substrate water molecules in the S_3 state based upon previous findings [56,58,59]. The slowdowns of both the lag and oxygen release phase during the S_3 to S_0 transition have been attributed to changes in the H-bond network that correspond to a suboptimal configuration of reactants and an associated entropic penalty for

crossing the activation barrier of the transition state [56]. The observation of slower water exchange in S_3 [59] has been suggested to be the result of the stabilization of water molecules due to altered H-bonding around the inserted substrate water, O_6/O_x. However, the mechanism of substrate exchange remains to be elucidated. As noted, D1/V185T and D1/V185N mutations replace the non-polar valine side chain with threonine or asparagine, which can introduce non-native hydrogen bonds to the putative O_6/O_x substrate and with water molecules (*e.g.* W3). This disruption likely affects both water binding and proton release.

The findings presented here underscore the central role of the H-bond network in modulating the LS-to-HS transition and subsequent steps in the Kok cycle. In Ca-PSII, the LS-to-HS transition is characterized by cooperative interactions among multiple protonatable groups, as evidenced by the best-fit value of n ~ 4.4 [30], although only one proton is ultimately released to the bulk solution [36]. Here, we can speculate that this cooperativity lowers the transition state barrier for proton release rather than stabilizing the deprotonated HS state itself. According to this view, the well-organized H-bond network facilitates a collective reorganization that creates an energetically favorable pathway for the LS-to-HS transition, ensuring efficient coupling of proton dynamics with substrate water insertion at the Mn_4CaO_5 cluster.

This may provide a view of some shared characteristics of proton transfer during both the $S_2 \rightarrow S_3$ and $S_3 \rightarrow S_0$ transitions. This $S_2 \rightarrow S_3$ transition also coincides with the critical insertion of W3—initially coordinated to Ca^{2+}—into the open coordination site on Mn1. This step is crucial for positioning W3 to become Ox, one of the two substrate waters for the water oxidation reaction. The timing and coordination of W3 insertion and its deprotonation is expected to be strongly influenced by the surrounding H-bond network. In the LS state, the network stabilizes W3 on Ca^{2+} in a protonated form, maintaining readiness for the subsequent catalytic steps. Upon insertion into Mn1 following the LS-to-HS transition, the reorganization of the H-bond network facilitates the deprotonation of W3, with the cooperative action lowering the activation barrier for this step and ensuring the system is primed for subsequent oxidation chemistry. Similarly, simulations in [73] emphasize that concerted proton shuffling between O6 and the waters W3 and W2, along with the extremely wide preorganization of an extended hydrogen bond network, is mandatory for $Tyr_Z^{\bullet}$ reduction in the $S_3 \rightarrow S_0$ transition. While a similar proton cooperativity to that seen in the formation of the S_2^{HS} state, such a cooperative transition on the HBN and its disruption by mutations or Sr-substitution could also account, for the slowdown of the $S_3 \rightarrow S_0$ transitions and help explain the increase in the entropic penalty and H/D effects previously observed for V185N. This insight aligns with the

idea that efficient catalysis requires not just local H-bond interactions but a globally integrated network capable of synchronizing proton and water dynamics across the system. Disruptions to this network, as seen in D1/V185 mutations and Sr^{2+} substitutions, likely hinder the necessary concerted movements, leading to slowed transitions and impaired water oxidation.

Consistent with this interpretation, we observe that the proton release during the $S_3 \rightarrow S_0$ transition in the D1/V185 mutants was primarily affected by the second of the two protons released during that transition. In contrast, the first proton release, which occurs rapidly following the formation of the tyrosine radical, $Tyr_Z^{\bullet}$, remains largely unaffected. This initial fast proton release is proposed to be linked to the electrostatic impact of uncompensated charge formation upon the effects of the formation of Tyr_ZOH-His190 → $Tyr_ZO^{\bullet}$-H^+His190 [70,71]. Functionally, this is proposed to occur to prepare Asp61D1 as a proton acceptor for the slower, second proton release from substrate water O6 [70,71,73,74]. The transient electric field during the $Tyr_ZO^{\bullet}$-H^+His190 state is calculated to promote proton transfer from W1 to Asp61, inducing rearrangements in the cluster of residues D1-Asp61, D1-Glu65, and D2-Glu312 into a configuration that facilitates rapid proton egress to the bulk [70,71,74]. The rapid exit of this proton is likely gated, preventing back-reactions. Once deprotonated, the cluster forms the base that accepts the proton from substrate water O6, facilitating the final electron transfer leading to O_2 formation [73]. The fact that the fast proton release remains unaffected by the mutation, while the second proton release is delayed, is consistent with the D1/V185 residue being distant from the fast proton release vector but positioned near the substrate water (O6), where deprotonation occurs. Thus, the delayed second proton release in the mutants is attributed to the disruption of the hydrogen-bonding network around O6, which slows the proton transfer pathway necessary for its deprotonation and the final stages of water oxidation.

Acknowledgements

This work has been in part supported by (i) the French Infrastructure for Integrated Structural Biology (FRISBI) ANR-10-INBS-05, (ii) the Labex Dynamo (ANR-11-LABX-0011-01), (iii) the JSPS-KAKENHI Grant in Scientific Research on Innovative Areas JP17H064351, JSPS-KAKENHI Grant 21H02447 and a grant from the US- National Science Foundation (MCB1716408). One of the PSII preparations used in this work was done by T. Tibiletti..

Legend of Figures

Figure 1: EPR spectra recorded at 8.6 K in WT PSII from *Synechocystis* 6803 (Panel A) and D1/V185N PSII from *Synechocystis* 6803 (Panel B). The black spectra were recorded in dark-adapted PSII. The red spectra were recorded after an illumination at 198 k for 5-10 s. The blue spectra are the "light"-*minus*-"dark" difference spectra. Instrument settings: [Chl] ~ 1.35 mg /ml; modulation amplitude, 25 G; microwave power, 20 mW; microwave frequency, 9.4 GHz; modulation frequency, 100 kHz. The unresolved spectral region at g ~ 2 (~ 3390 gauss) corresponds to the saturated signal from $Tyr_D^{\bullet}$.

Figure 2: Time-courses of the absorption changes of bromocresol purple at 575 nm in PsbA3-PSII (Panel A) and PsbA3/V185T-PSII (Panel B) from *T. vestitus* after the 1st flash (black points), the 2nd flash (red points), the 3rd flash (blue points), and the 4th flash (green points). Panel C; time-courses of the absorption change differences 440 nm-*minus*-424 nm after the first flash (black), the second flash (red), the third flash (blue), and the fourth flash (green) given to dark-adapted PsbA3/V185T-PSII in the presence of 100 μM PPBQ with flashes spaced 400 ms apart.

Figure 3: Kinetics of flash-induced absorption changes measured at 432 nm in PsbA3-PSII (black), and PsbA3/V185T-PSII (red) from *T. vestitus* after the 1st flash (Panel A), the 2nd flash (Panel B), the 3rd flash (Panel C) and the 4th flash (Panel D). The amplitudes of the kinetics were normalized to OD673nm = 1.75 (a Chl concentration of ~ 25 μg/ml). 100 μM PPBQ was added before the measurements were taken. Panel E shows the amplitude of the ΔI/I at 20 ns, and at 432 nm, after each flash of the sequence with flashes spaced 400 ms apart.

References

[1] D. Shevela, J.F. Kern, G. Govindjee, J. Messinger, Solar energy conversion by photosystem II: principles and structures, Photosynth. Res. 156 (2023) 279-307. https://doi.org/10.1007/s11120-022-00991-y

[2] Y. Umena, K. Kawakami, J.-R. Shen, N. Kamiya, Crystal structure of oxygen evolving Photosystem II at a resolution of 1.9 angstrom, Nature 473 (2011) 55–60. https://doi.org/10.1038/nature09913

[3] H. Ago, H. Adachi, Y. Umena, T. Tashiro, K. Kawakami, N. Kamiya, L.R. Tian, G.Y. Han, T.Y. Kuang, Z.Y. Liu, F.J. Wang, H.F. Zou, I. Enami, M. Miyano, J.-R. Shen, Novel features of eukaryotic photosystem II revealed by its crystal structure analysis from a red alga, J. Biol. Chem. 291 (2016) 5676–5687. https://doi.org/10.1074/jbc.M115.711689

[4] C.J. Gisriel, J. Wang, J. Liu, D.A. Flesher, K.M. Reiss, H.-L. Huang, K.R. Yang, W.H. Armstrong, M.R. Gunner, V.S. Batista, R.J. Debus, G.W. Brudvig, High resolution cryo-electron microscopy structure of photosystem II from the mesophilic cyanobacterium, *Synechocystis* sp. PCC 6803, Proc. Natl. Acad. Sci. U. S. A. 119 (2022), e2116765118. https://doi.org/10.1073/pnas.2116765118

[5] A.R. Holzwarth, M.G. Müller, M. Reus, M. Nowaczyk, J. Sander, M. Rögner, Kinetics and mechanism of electron transfer in intact Photosystem II and in the isolated reaction center: pheophytin is the primary electron acceptor, Proc. Natl. Acad. Sci. U. S. A. 103 (2006) 6895–6900. https://doi.org/10.1073/pnas.0505371103

[6] F. Muh, M. Plockinger, T. Renger, Electrostatic asymmetry in the reaction center of Photosystem II, J. Phys. Chem. Lett. 8 (2017) 850–858. https://doi.org/10.1021/acs.jpclett.6b02823

[7] A. Sirohiwal, D.A. Pantazis, Reaction center excitation in Photosystem II: From multiscale modeling to functional principles, Acc. Chem. Res. 56 (2023) 2921−2932. https://doi.org/10.1021/acs.accounts.3c00392

[8] D.J. Vinyard, G.M. Ananyev, G.C. Dismukes, Photosystem II: the reaction center of oxygenic photosynthesis, Annu. Rev. Biochem. 82 (2013) 577–606. https://10.1146/annurev-biochem-070511-100425

[9] J. Yano, J. Kern, V.K. Yachandra, Structure function studies of Photosystem II using X-ray free electron lasers, Annu. Rev. Biophys. 53 (2024)343–65. https://doi.org/10.1146/annurev-biophys-071723-102519

[10] W. Lubitz D.A. Pantazis N. Cox , Water oxidation in oxygenic photosynthesis studied by magnetic resonance techniques, FEBS Lett. 597 (2023) 6–29. https://doi.org/10.1002/1873-3468.14543

[11] N. Oliver, A.P. Avramov, D.J. Nürnberg, H. Dau, R.L. Burnap, From manganese oxidation to water oxidation: assembly and evolution of the water-splitting complex in photosystem II, Photosynth. Res. 152 (2022) 107–133. https://doi.org/10.1007/s11120-022-00912-z

[12] T. Oliver, T.D. Kim, J.P. Trinugroho, V. Cord´on-Preciado, N. Wijayatilake, A. Bhatia, A.W. Rutherford, T. Cardona, The evolution and evolvability of photosystem II, Annu. Rev. Plant Biol. 74 (2023) 24.1–24.33, https://doi.org/10.1146/annurev-arplant-070522-062509

[13] P. Joliot, Period-four oscillations of the flash-induced oxygen formation in photosynthesis, Photosynth. Res. 76 (2003) 65–72. https://doi.org/10.1023/A:1024946610564

[14] B. Kok, B. Forbush, M. McGloin, Cooperation of charges in photosynthetic O_2 evolution–I. A linear four step mechanism, Photochem. Photobiol. 11 (1970) 457–475. https://doi.org/10.1111/j.1751-1097.1970.tb06017.x

[15] J. Kern, R. Chatterjee, I.D. Young, F.D. Fuller, L. Lassalle, M. Ibrahim, S. Gul, T. Fransson, A.S. Brewster, R. Alonso-Mori, R. Hussein, M. Zhang, L. Douthit, C. de Lichtenberg, M. Hon Cheah, D. Shevela, J. Wersig, I. Seuffert, D. Sokaras, E. Pastor, C. Weninger, T. Kroll, R.G. Sierra, P. Aller, A. Butryn, A.M. Orville, M. Liang, A. Batyuk, J.E. Koglin, S. Carbajo, S. Boutet, N.W. Moriarty, J.M. Holton, H. Dobbek, P.D. Adams, U. Bergmann, N.K. Sauter, A. Zouni, J. Messinger, J. Yano, V.K. Yachandra, Structures of the intermediates of Kok's photosynthetic water oxidation clock, Nature 563 (2018) 421. https://doi.org/10.1038/s41586-018-0681-2

[16] A. Bhowmick, P.S. Simon, I. Bogacz, R. Hussein, M. Zhang, H. Makita, M. Ibrahim, R. Chatterjee, M.D. Doyle, M. Hon Cheah, P. Chernev, F.D. Fuller, T. Fransson, R. Alonso-Mori, A.S. Brewster, N.K. Sauter, U. Bergmann, H. Dobbek, A. Zouni, J. Messinger, J. Kern, V.K. Yachandra, J. Yano, Going around the Kok cycle of the water oxidation reaction with femtosecond X-ray crystallography, IUCrJ 10 (2023) 642–655. https://doi.org/10.1107/S2052252523008928

[17] H. Li, Y. Nakajima, E. Nango, S. Owada, D. Yamada, K. Hashimoto, F. Luo, R. Tanaka, F. Akita, K. Kato, J. Kang, Y. Saitoh, S. Kishi, H. Yu, N. Matsubara, H. Fujii, M. Sugahara, M. Suzuki, T. Masuda, T. Kimura, T. Nguyen Thao, S. Yonekura, L-J. Yu, T. Tosha, K. Tono, Y. Joti, T. Hatsui, M. Yabashi, M. Kubo, S. Iwata, H. Isobe, K. Yamaguchi, M. Suga, J-R. Shen,

Oxygen-evolving photosystem II structures during S1–S2–S3 transitions, Nature 626 (2024) 670–677. https://doi.org/10.1038/s41586-023-06987-5

[18] C. de Lichtenberg, L. Rapatskiy, M. Reus, E. Heyno, A. Schnegg, M.M. Nowaczyk, W. Lubitz, J. Messinger, N. Cox, Assignment of the slowly exchanging substrate water of nature's water-splitting cofactor, Proc. Natl. Acad. Sci. U. S. A. 121 (2024) e2319374121. https://doi.org/10.1073/pnas.2319374121

[19] S.L. Dexheimer, M.P. Klein, Detection of a paramagnetic intermediate in the S_1 state of the photosynthetic oxygen-evolving complex, J. Am. Chem. Soc. 114 (1992) 2821–2826. https://doi.org/10.1021/ja00034a010

[20] T. Yamauchi, H. Mino, T. Matsukawa, A. Kawamori, T.-A. Ono, Parallel polarization electron paramagnetic resonance studies of the S_1-state manganese cluster in the photosynthetic oxygen-evolving system, Biochemistry 36 (1997) 7520–7526. https://doi.org/10.1021/bi962791g

[21] K.A. Campbell, J.M. Peloquin, D.P. Pham, R.J. Debus, R.D. Britt, Parallel polarization EPR detection of an S1-State "Multiline" EPR signal in Photosystem II particles from *Synechocystis* sp. PCC 6803, J. Am. Chem. Soc. 120 (1998) 447–448. https://doi.org/10.1021/ja972693y

[22] M. Drosou, G. Zahariou, D.A. Pantazis, Orientational Jahn-Teller isomerism in the dark-stable state of nature's water oxidase, Angew. Chem. Int. Ed. 60 (2021,13493–13499. https://doi.org/10.1002/anie.202103425

[23] G.C. Dismukes, Y. Siderer, Intermediates of a polynuclear manganese center involved in photosynthetic oxidation of water, Proc. Natl. Acad. Sci. U. S. A. 78 (1981) 274–278. https://doi.org/10.1073/pnas.78.1.274

[24] J.M. Peloquin, K.A. Campbell, D.W. Randall, M.A. Evanchik, V.L. Pecoraro, W. H. Armstrong, R.D. Britt, Mn-55 ENDOR of the S2-state multiline EPR signal of photosystem II: implications on the structure of the tetranuclear mn cluster, J. Am. Chem. Soc. 122 (2000) 10926–10942. https://doi.org/10.1021/ja002104f

[25] N. Cox, L. Rapatskiy, J.-H. Su, D.A. Pantazis, M. Sugiura, L. Kulik, P. Dorlet, A.W. Rutherford, F. Neese, A. Boussac, W. Lubitz, J. Messinger, Effect of Ca^{2+}/Sr^{2+} substitution on the electronic structure of the oxygen-evolving complex of photosystem II: a combined multifrequency EPR, mn-55-ENDOR, and DFT study of the S_2 state, J. Am. Chem. Soc. 133 (2011) 3635–3648. https://doi.org/10.1021/ja110145v

[26] J.-L. Zimmermann, A.W. Rutherford, Electron paramagnetic resonance studies of the oxygen-evolving enzyme of photosystem II, Biochim. Biophys. Acta 767 (1984) 160–167, https://doi.org/10.1016/0005-2728(84)90091-4

[27] J.L. Casey, K. Sauer, Electron paramagnetic resonance detection of a cryogenically photogenerated intermediate in photosynthetic oxygen evolution, Biochim. Biophys. Acta 767 (1984) 21–28. https://doi.org/10.1016/0005-2728(84)90075-6

[28] A. Boussac, S. Un, O. Horner, A.W. Rutherford, High spin states ($S \geq 5/2$) of the photosystem II manganese complex, Biochemistry 37 (1998) 4001–4007. https://doi.org/10.1021/bi9728710

[29] A. Boussac, H. Kuhl, S. Un, M. Rögner, A.W. Rutherford, Effect of near-infrared light on the S_2-state of the manganese complex of photosystem II from *Synechococcus elongatus*, Biochemistry 37 (1998) 8995–9000. https://doi.org/10.1021/bi980195b

[30] A. Boussac, I. Ugur, A. Marion, M. Sugiura, V.R.I. Kaila, A.W. Rutherford, The low spin - high spin equilibrium in the S_2-state of the water oxidizing enzyme, Biochim. Biophys. Acta 2018 (1859) 342–356. https://doi.org/10.1016/j. bbabio.2018.02.010.

[31] A. Boussac, Temperature dependence of the high-spin S_2 to S_3 transition in photosystem II: mechanistic consequences, Biochim. Biophys. Acta 2019 (1860) 508–518. https://doi.org/10.1016/j.bbabio.2019.05.001

[32] D.A. Pantazis, W. Ames, N. Cox, W. Lubitz, F. Neese, Two interconvertible structures that explain the spectroscopic properties of the oxygen-evolving complex of photosystem II in the S_2 state, Angew. Chem. Intl. Ed. 51 (2012) 9935–9940. https://doi.org/10.1002/anie.201204705

[33] T.A. Corry, P.J. O'Malley, Proton isomers rationalize the high- and low-spin forms of the S2 state intermediate in the water-oxidizing reaction of photosystem II, J. Phys. Chem. Lett. 10 (2019) 5226–5230. https://doi.org/10.1021/acs. jpclett.9b01372

[34] T.A. Corry, P.J. O'Malley, Molecular identification of a high-spin deprotonated intermediate during the S_2 to S_3 transition of nature's water-oxidizing complex, J. Am. Chem. Soc. 142 (2020) 10240–10243. https://doi.org/10.1021/jacs.0c01351

[35] M. Barchenko, P.J. O'Malley, A reappraisal of the S_2 state of nature's water oxidizing complex in its low and high spin forms, J. Phys. Chem. Lett. 15 (2024) 5883−5886. https://doi.org/10.1021/acs.jpclett.4c00997

[36] A. Boussac, M. Sugiura, J. Sellés, Probing the proton release by Photosystem II in the S_1 to S_2 high-spin transition, Biochim. Biophys. Acta 1863 (2022), 148546. https://doi.org/10.1016/j.bbabio.2022.148546

[37] Y. Sanakis, J. Sarrou, G. Zahariou, V. Petrouleas, Q-band electron paramagnetic resonance studies of the S_3 state of the OEC of Photosystem II, in: J.F. Allen, E. Gantt, J.H. Golbeck, B. Osmond (Eds.), Photosynthesis. Energy From the Sun, Springer, Dordrecht, 2008. https://doi.org/10.1007/978-1-4020-6709-9_108

[38] A. Boussac, M. Sugiura, A.W. Rutherford, P. Dorlet, Complete EPR spectrum of the S_3-state of the oxygen-evolving photosystem II, J. Am. Chem. Soc. 131 (2009) 5050–5051. https://doi.org/10.1021/ja900680t

[39] N. Cox, M. Retegan, F. Neese, D.A. Pantazis, A. Boussac, W. Lubitz, Electronic structure of the oxygen evolving complex in photosystem II prior to O-O bond formation, Science 345 (2014) 804–808. https://doi.org/10.1126/science.1254910

[40] A. Boussac, A.W. Rutherford, M. Sugiura, Electron transfer pathways from the S_2-states to the S_3-states either after a Ca^{2+}/Sr^{2+} or a Cl^-/I^- exchange in Photosystem II from *Thermosynechococcus elongatus*, Biochim. Biophys. Acta 1847 (2015) 576–586. http://dx.doi.org/10.1016/j.bbabio.2015.03.006

[41] D.A. Marchiori, R.J. Debus, R.D. Britt, Pulse EPR spectroscopic characterization of the S_3 state of the oxygen-evolving complex of photosystem II isolated from *Synechocystis*, Biochemistry 59 (2020) 4864–4872. https://doi.org/10.1021/acs.biochem.0c00880

[42] G. Zahariou, N. Ioannidis, Y. Sanakis, D.A. Pantazis, Arrested substrate binding resolves catalytic intermediates in higher-plant water oxidation, Angew. Chem. Intl. Ed. 60 (2020) 3156–3162. https://doi.org/10.1002/anie.202012304

[43] M. Chrysina, E. Heyno, Y. Kutina, M. Reus, H. Nilsson, M.M. Nowaczyk, S. DeBeer, F. Neese, J. Messinger, W. Lubitz, N. Cox, Five-coordinate Mn^{IV} intermediate in the activation of nature's water splitting cofactor, Proc. Nat. Aca. Sci. USA 116 (2019) 16841–16846. https://doi.org/10.1073/pnas.1817526116

[44] K.G.V. Havelius, J.-H. Su, Y. Feyziyev, F. Mamedov, S. Styring, Spectral resolution of the split EPR signals induced by illumination at 5 K from the S_1, S_3, and S_0 states in photosystem II, Biochemistry 45 (2006) 9279–9290. https://doi.org/10.1021/bi060698e

[45] A. Boussac, M. Sugiura, T.-L. Lai, A.W. Rutherford, Low-temperature photochemistry in Photosystem II from *Thermosynechococcus elongatus* induced by visible and near-infrared light, Philos. Trans. R. Soc. London, Ser. B 363 (2008) 1203–1210. https://doi.org/10.1098/rstb.2007.2216

[46] V. Krewald, F. Neese, D.A. Pantazis, Implications of structural heterogeneity for the electronic structure of the final oxygen-evolving intermediate in photosystem II, J. Inorg. Biochem. 199 (2019), 110797. https://doi.org/10.1016/j.jinorgbio.2019.110797

[47] M. Drosou, D.A. Pantazis, Redox isomerism in the S_3 state of the oxygen-evolving complex resolved by coupled cluster theory, Chem. Eur. J. 27 (2021) 12815–12825. https://doi.org/10.1002/chem.202101567

[48] H. Isobe, M. Shoji, T. Suzuki, J.-R. Shen, Spin, valence, and structural isomerism in the S_3 state of the oxygen-evolving complex of photosystem II as a manifestation of multimetallic cooperativity, J. Chem. Theory Comput. 15 (2019) 2375–2391. https://doi.org/10.1021/acs.jctc.8b01055

[49] M. Chrysina, M. Drosou, R.G. Castillo, M. Reus, F. Neese, V. Krewald, D.A. Pantazis, S. DeBeer, Nature of S-states in the oxygen-evolving complex resolved by high-energy resolution fluorescence detected X-ray absorption spectroscopy, J. Am. Chem. Soc. 145 (2023) 25579–25594. https://doi.org/10.1021/jacs.3c06046

[50] A. Klauss, M. Haumann, H. Dau, Seven steps of alternating electron and proton transfer in photosystem II water oxidation traced by time-resolved photothermal beam deflection at improved sensitivity, J. Phys. Chem. B 119 (2015) 2677–2689. https://doi.org/10.1021/jp509069p

[51] I. Zaharieva, H. Dau, M. Haumann, Sequential and coupled proton and electron transfer events in the $S_2 \rightarrow S_3$ transition of photosynthetic water oxidation revealed by time-resolved X-ray absorption spectroscopy, Biochemistry 55 (2016) 6996–7004. https://doi.org/10.1021/acs.biochem.6b01078

[52] Y. Okamoto, Y. Shimada, R. Nagao, T. Noguchi, Proton and water transfer pathways in the $S_2 \rightarrow S_3$ transition of the water-oxidizing complex in photosystem II: time-resolved infrared analysis of the effects of D1–N298A mutation and NO_3-substitution, J. Phys. Chem. B 125 (2021) 6864–6873. https://doi.org/10.1021/acs.jpcb.1c03386

[53] S.M. Mausle, A. Abzaliyeva, P. Greife, P.S. Simon, R. Perez, Y. Zilliges, H. Dau, Activation energies for two steps in the $S_2 \rightarrow S_3$ transition of photosynthetic water oxidation from time-resolved single-frequency infrared spectroscopy, J. Chem. Phys. 153 (2020) 215101. https://doi.org/10.1063/5.0027995

[54] A. Boussac, J. Sellés, M. Sugiura, What can we still learn from the electrochromic band-shifts in photosystem II? Biochim. Biophys. Acta 1861 (2020), 148176. https://doi.org/10.1016/j.bbabio.2020.148176

[55] M. Ibrahim, T. Fransson, R. Chatterjee, M.H. Cheah, R. Hussein, L. Lassalle, K.D. Sutherlin, I.D. Young, F.D. Fuller, S. Gul, I.S. Kim, P.S. Simon, C. de Lichtenberg, P. Chernev, I. Bogacz, C.C. Pham, A.M. Orville, N. Saichek, T. Northen, A. Batyuk, S. Carbajo, R. Alonso-Mori, K. Tono, S. Owada, A. Bhowmick, R. Bolotovsky, D. Mendez, N.W.

Moriarty, J.M. Holton, H. Dobbek, A.S. Brewster, P.D. Adams, N. K. Sauter, U. Bergmann, A. Zouni, J. Messinger, J. Kern, V.K. Yachandra, J. Yano, Untangling the sequence of events during the $S_2 \rightarrow S_3$ transition in photosystem II and implications for the water oxidation mechanism, Proc. Natl. Acad. Sci. U. S. A.117 (2020) 12624–12635. https://doi.org/10.1073/pnas.2000529117

[56] H. Bao, R.L. Burnap, Structural rearrangements preceding dioxygen formation by the water oxidation complex of Photosystem II, Proc. Natl. Acad. Sci. U. S. A. 112 (2015) 6139-6147. https://doi.org/10.1073/pnas.1512008112

[57] P.L. Dilbeck, H. Bao, C.L. Neveu, R.L. Burnap, Perturbing the water cavity surrounding the manganese cluster by mutating the residue D1-Valine 185 has a strong effect on the water oxidation mechanism of Photosystem II, Biochemistry 52 (2013) 6824–6833. https://doi.org/10.1021/bi400930g

[58] C.J. Kim, H. Bao, R.L. Burnap, R.J. Debus, Impact of D1-V185 on the water molecules that facilitate O_2 formation by the catalytic Mn_4CaO_5 cluster in Photosystem II, Biochemistry 57 (2018) 4299–4311. https://doi.org/10.1021/acs.biochem.8b00630

[59] C. de Lichtenberg, A.P. Avramov, M.Q. Zhang, F. Mamedov, R.L. Burnap, J. Messinger, The D1-V185N mutation alters substrate water exchange by stabilizing alternative structures of the Mn4Ca-cluster in photosystem II, Biochim. Biophys. Acta 1862 (2021) 148319. https://doi.org/10.1016/j.bbabio.2020.148319

[60] M. Sugiura, T. Tibiletti, I. Takachi, Y. Hara, S. Kanawaku, J. Sellés, A. Boussac, Probing the role of Valine 185 of the D1 protein in the Photosystem II oxygen evolution, Biochim. Biophys. Acta 1859 (2018) 1259–1273. https://doi.org/10.1016/j.bbabio.2018.10.003

[61] M.J. Schilstra, F. Rappaport, J.H. Nugent, C.J. Barnett, D.R. Klug, Proton/hydrogen transfer affects the S state-dependent microsecond phases of P_{680}^+ reduction during water splitting, Biochemistry 37 (1998) 3974–3981. https://doi.org/10.1021/bi9713815

[62] P. Kuhn, H. Eckert, H.J. Eichler, G. Renger, Analysis of the P_{680}^+ reduction pattern and its temperature dependence in oxygen evolving PSII core complexes from a thermophilic cyanobacteria and higher plants, Phys. Chem. Chem. Phys. 6 (2004) 4838–4843. https://doi.org/10.1039/b407656g

[63] G. Christen, G. Renger, The role of hydrogen bonds for the multiphasic P_{680}^+ reduction by Y_Z in photosystem II with intact oxygen evolution capacity: analysis of kinetic H/D isotope exchange effects, Biochemistry 38 (1999) 2068–2077. https://doi.org/10.1021/bi982188t

[64] D. Béal, F. Rappaport, P. Joliot, A new high-sensitivity 10-ns time-resolution spectrophotometric technique adapted to in vivo analysis of the photosynthetic apparatus, Rev. Sci. Instrum. 70 (1999) 202–207. https://doi.org/10.1063/1.1149566

[65] M. Sugiura, T. Taniguchi, N. Tango, M. Nakamura, J. Sellés, A. Boussac, Probing the role of arginine 323 of the D1 protein in photosystem II function, Physiol. Plant. 171 (2021) 183–199. https://doi.org/10.1111/ppl.13115

[66] J-L. Zimmermann, A.W. Rutherford, Photoreductant-induced oxidation of Fe^{2+} in the electron-acceptor complex of Photosystem II, Biochim. Biophys. Acta 851 (1986) 416–423. https://doi.org/10.1016/0005-2728(86)90078-2

[67] C. Fufezan, C. Zhang, A. Krieger-Liszkay, A.W. Rutherford, Secondary quinone in Photosystem II of *Thermosynechococcus elongatus*: Semiquinone−Iron EPR signals and temperature dependence of electron transfer, Biochemistry 44 (2005) 12780–12789. https://doi.org/10.1021/bi051000k

[68] F. Rappaport, J. Lavergne, Proton release during successive oxidation steps of the photosynthetic water oxidation process - stoichiometries and pH-dependence, Biochemistry 30 (1991) 10004–10012. https://doi.org/10.1021/bi00105a027

[69] K. Brettel, E. Schlodder, H.T. Witt, Nanosecond reduction kinetics of photooxidized chlorophyll-a_{II} (P-680) in single flashes as a probe for the electron pathway, H^+-release and charge accumulation in the O_2-evolving complex, Biochim. Biophys. Acta 766 (1984) 403–415. https://doi.org/10.1016/0005-2728(84)90256-1

[70] F. Allgöwer, A.P. Gamiz-Hernandez, A.W. Rutherford, V.R.I. Kaila, Molecular principles of redox-coupled protonation dynamics in Photosystem II, J. Am. Chem. Soc. 144 (2022) 7171–7180. https://doi.org/10.1021/jacs.1c13041

[71] F. Allgöwer, M.C. Pöverlein, A.W. Rutherford, V.R.I. Kaila, Mechanism of proton release during water oxidation in Photosystem II. BioRxiV https://doi.org/10.1101/2024.07.03.602004

[72] A. Boussac, Temperature dependence of the high-spin S_2 to S_3 transition in Photosystem II: Mechanistic consequences, Biochim. Biophys. Acta 1860 (2019) 508–519. https://doi.org/10.1016/j.bbabio.2019.05.001

[73] H. Dau, P. Greife, Applicability of transition state theory to the (proton-coupled) electron transfer in photosynthetic water oxidation with emphasis on the entropy of activation, Inorganics 11 (2023) 389. https://doi.org/10.3390/inorganics11100389

[74] T. Noguchi, Mechanism of proton transfer through the D1-E65/D2-E312 gate during photosynthetic water oxidation, J. Phys. Chem. B 128 (2024) 1866−1875. https://doi.org/10.1021/acs.jpcb.3c07787

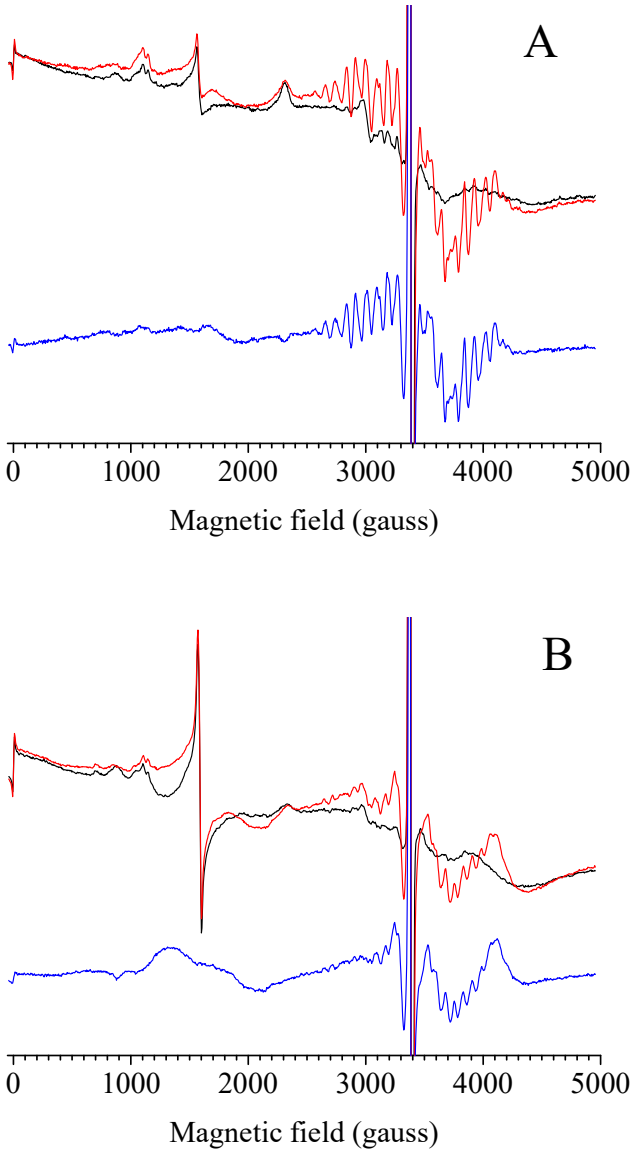
A
0
1000
2000
3000
4000
5000
Magnetic field (gauss)
B
0
1000
2000
3000
4000
5000
Magnetic field (gauss)

Fig. 1

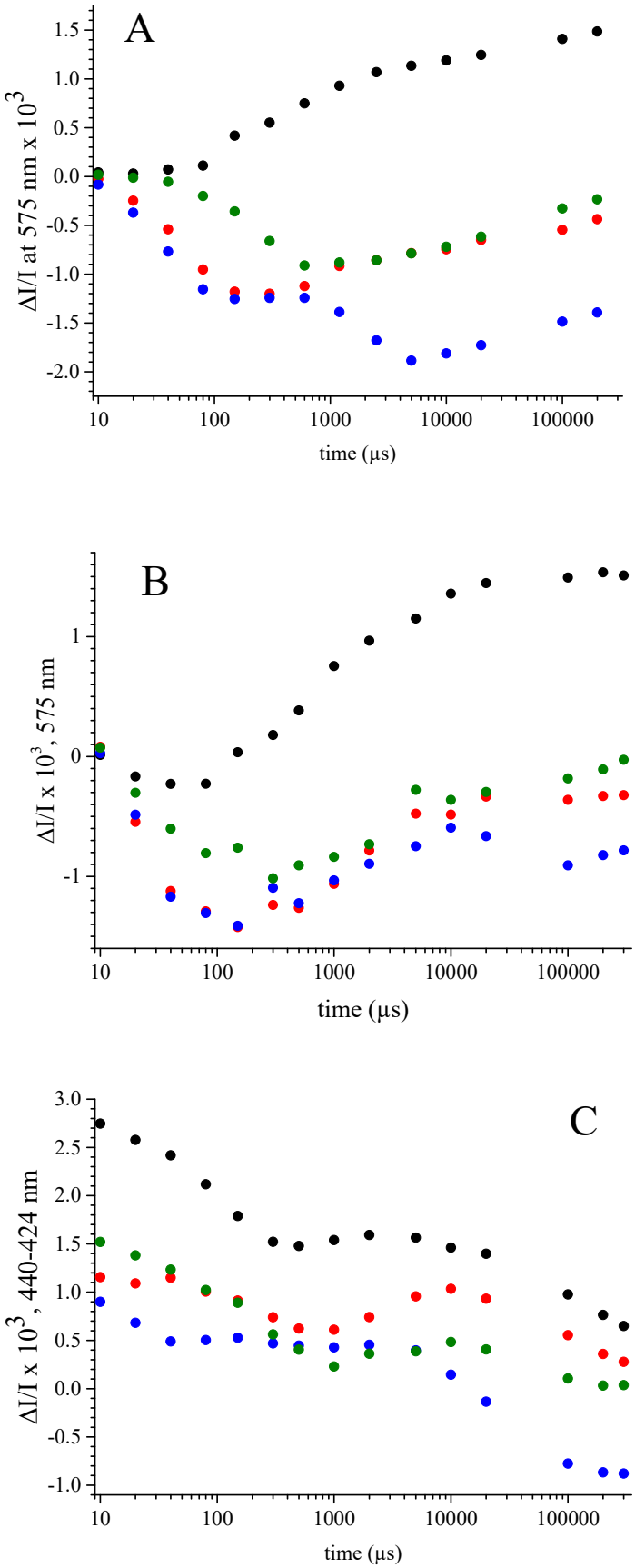
A
ΔI/I at 575 nm x 10^3
1.5
1.0
0.5
0.0
-0.5
-1.0
-1.5
-2.0
10
100
1000
10000
100000
time (μs)
B
ΔI/I x 10^3, 575 nm
1
0
-1
10
100
1000
10000
100000
time (μs)
C
ΔI/I x 10^3, 440-424 nm
3.0
2.5
2.0
1.5
1.0
0.5
0.0
-0.5
-1.0
10
100
1000
10000
100000
time (μs)

Fig. 2

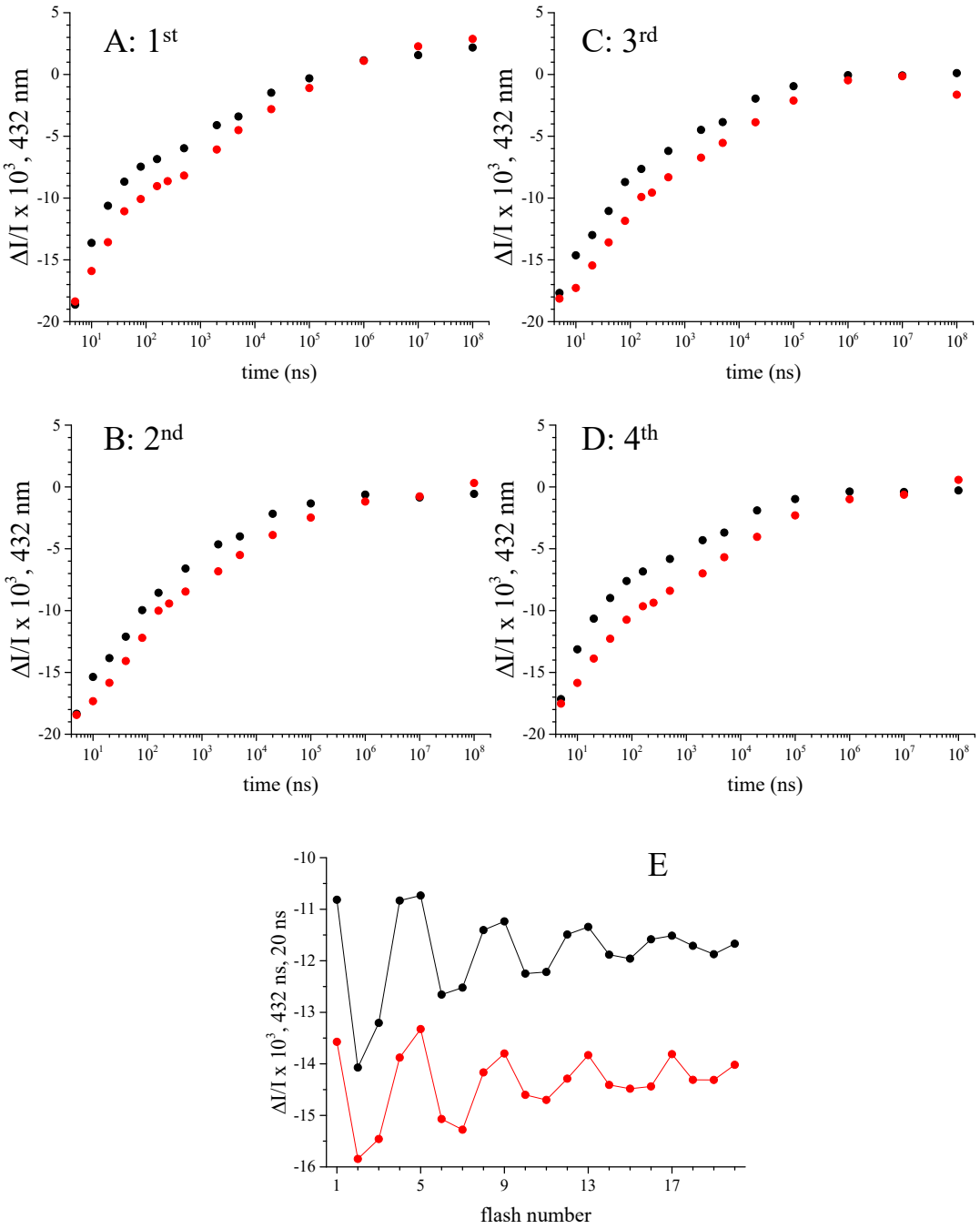
A: 1st
B: 2nd
C: 3rd
D: 4th
E
ΔI/I x 10^3, 432 nm
time (ns)
ΔI/I x 10^3, 432 ns, 20 ns
flash number

Fig. 3